Multilayer Graphene Terahertz Plasmonic Structures for

Enhanced Frequency Tuning Range

Geng Li, Viacheslav Semenenko, Vasili Perebeinos, Peter Q. Liu*

Department of Electrical Engineering, University at Buffalo, the State University of New York,

Buffalo, New York 14260, United States

Abstract

Graphene plasmonics has recently found a variety of applications in terahertz photonic devices.

High spatial confinement and large frequency tunability are two key advantages of graphene

plasmonics. Nevertheless, the frequency tuning range of plasmonic devices employing single-layer

graphene is ultimately limited by its carrier density tuning range. Here, we demonstrate that the

frequency tuning range of graphene-based plasmonic devices can be further extended by

employing multilayer graphene structures. Both our experimental investigation and theoretical

calculation show that the frequency tuning range of gate-controlled graphene plasmonic resonators

can be significantly enhanced by employing two or three layers of stacked graphene, which is a

result of the carrier distributions in multiple layers leading to higher total optical conductivity.

However, contrary to the previous prediction, stacking even more graphene layers yields little

additional benefit, as the interlayer charge screening effect leads to insignificant gate-induced

carrier density in additional graphene layers. Our findings provide new insights for designing and

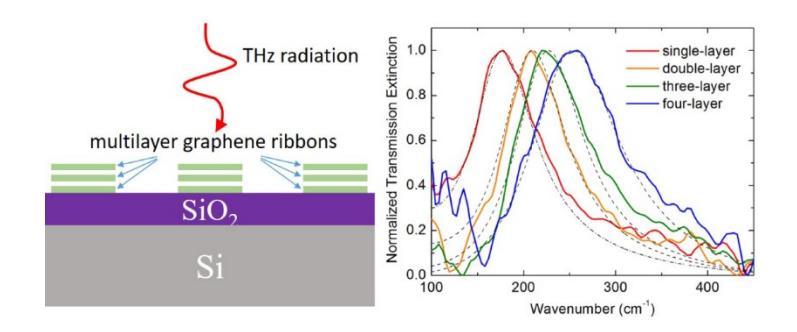
optimizing graphene-based plasmonic structures for various photonic device applications, such as

modulators, sensors and detectors.

Keywords: plasmonics, multilayer graphene, terahertz, metasurface, frequency tuning.

1

TOC Graphic



Text

Graphene, since its discovery, has attracted extensive research and development efforts in both academia and industry due to its various interesting material properties and potential applications.² One of the most attractive properties of graphene for photonics is its ability to support plasmons, i.e., collective oscillations of two-dimensional (2D) massless electrons, which exhibit distinct characteristics from those of conventional 2D electron gases.³⁻⁷ Thanks to its high spatial confinement of electromagnetic waves, graphene plasmon has become a suitable platform for enhancing light-matter interactions in the mid-infrared to terahertz (THz) spectral region,⁵ which may in turn benefit a broad range of photonic and optoelectronic device applications.⁸⁻¹³ The research field of graphene plasmonics has experienced rapid progress in recent years. Graphene plasmons in a variety of structures and heterostructures have been imaged using near-field scanning optical microscopy for understanding their properties and fundamental limits.¹⁴⁻¹⁸ A variety of tunable resonant graphene plasmonic structures have been demonstrated. ^{6,19-24} Graphene plasmonic structures have also been employed in a broad range of device applications such as optical modulators, 11 biosensors, 12 and photodetectors. 13 However, most of these previous work focused on plasmonic structures made of single-layer graphene, whereas only a small number of Stacks of multiple layers of randomly oriented graphene and insulating polymer films have been utilized for realizing THz plasmonic resonators which exhibited strong transmission extinction. ¹⁹ Interesting effects associated with Bernal-stacking bilayer graphene plasmonic structures have also been studied. ^{25,26} Moreover, double-layer graphene structures (with random interlayer alignment) fabricated by two successive transfer of single-layer graphene without any insulating spacer in between have been investigated, ^{27,28} which showed higher tuning range of plasmonic resonance frequency and enhanced transmission extinction compared to those of single-layer graphene structures of the same dimensions. In the previous report, it was assumed that the electrostatic gating induces an equal change in the Fermi energy of each graphene layer, which in theory would lead to the resonance frequency of an N-layer graphene plasmonic resonator reaching up to $\sqrt[4]{N}$ times that of the corresponding single-layer graphene structure. ²⁸ However, such multilayer graphene plasmonic structures with gate-controlled frequency tunability have not been more systematically studied yet.

Here, we present a systematic study of gate-controlled multilayer graphene ribbon arrays which exhibit tunable plasmonic resonances in the THz region. We show that the frequency tuning range of the graphene plasmonic resonances are significantly enhanced for both double-layer and three-layer graphene structures, but little additional benefit is achieved by employing even more layers. Our theoretical calculation shows that this is mainly because the interlayer charge screening effect leads to a considerably non-equal distribution of gate-tunable carrier densities in different graphene layers. The plasmonic resonance frequency of a multilayer graphene structure is mostly determined by the carrier density distribution in the first two or three layers, whereas the gate-induced carrier density in the *j*-th layer is insignificant for $j \ge 4$. Our theoretical calculation

and experimental observation are in good agreement. The findings presented here provide new insights for developing an optimal strategy to expand the graphene plasmonics platform by employing multilayer graphene structures, which may be utilized to further enhance various lightmatter interactions for different photonic and optoelectronic device applications, such as modulators, sensors and detectors.

We choose graphene ribbons for this study because they have been shown to exhibit relatively strong THz plasmonic resonances. Nevertheless, the findings presented here should also apply to graphene structures of other geometries. Figure 1(a) shows the schematic of the investigated plasmonic structures. To achieve stacking of multiple layers of graphene, we repeatedly transfer large-area single-layer graphene onto a doped silicon substrate with a \sim 300 nm silicon dioxide layer on the surface. The single-layer graphene (acquired from Graphene Square) was synthesized on copper foil using chemical vapor deposition. The stacked graphene layers have random orientations and hence no band structure modification is expected. After the transfer process, we pattern periodic arrays of graphene ribbons with \sim 1 μ m ribbon width and 2 μ m periodicity using photolithography followed by oxygen plasma etching. Metal contacts (Ti/Au) to graphene are then deposited using an electron beam evaporator. Multiple graphene ribbon array samples with the number of graphene layers ranging from 1 to 4 are fabricated. The doped Si substrate functions as a back-gate for these multilayer graphene structures. Figure 1(b) shows a scanning electron microscopy (SEM) image of a fabricated three-layer graphene ribbon array.

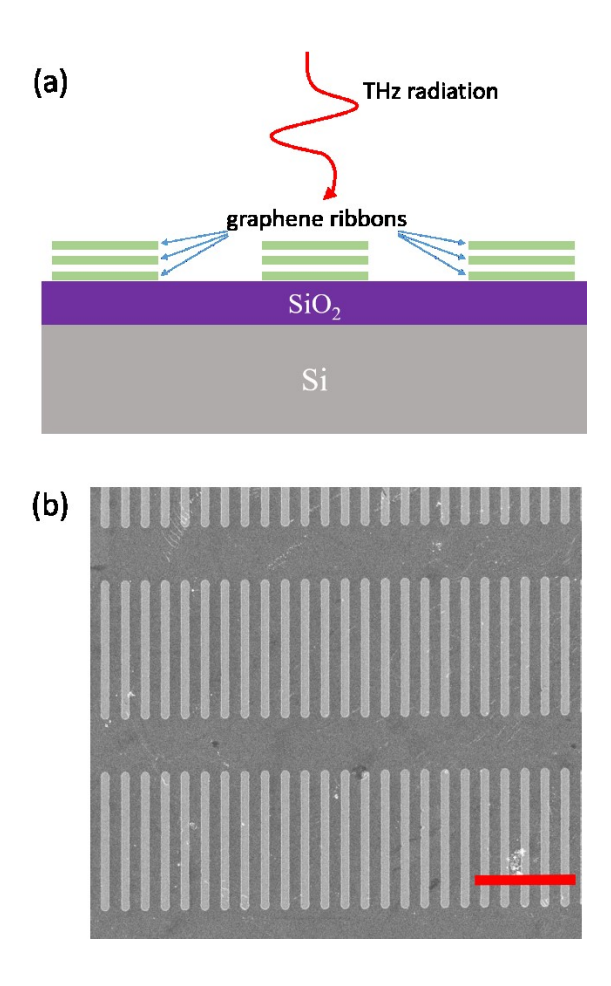


Figure 1. (a) Schematic of the investigated multilayer graphene ribbon arrays on SiO₂/Si substrate. (b) SEM image of a fabricated three-layer graphene ribbon array with a ribbon width of \sim 1.15 μm and a periodicity of 2 μm. Scale bar is 10 μm.

We characterize the carrier density dependent plasmonic resonances of the fabricated multilayer graphene ribbons using a Fourier transform infrared spectrometer (FTIR, model Bruker Vertex 70v). The samples are placed in the vacuum chamber of the FTIR during the measurements. Transmission spectra (T) of each sample at various back-gate voltages are measured. The transmission extinction spectra are then calculated as $1 - T/T_{\rm CNP}$, where $T_{\rm CNP}$ is the transmission spectrum when the graphene structure is biased at the charge neutrality point (CNP) gate voltage

 $V_{\rm CNP}$. Resonance peaks in these transmission extinction spectra correspond to enhanced absorption at the graphene plasmonic resonances. Figure 2(a)-(b) show the transmission extinction spectra of a three-layer graphene ribbon array at various gate voltages ($\Delta V_{\text{gate}} = |V_{\text{gate}} - V_{\text{CNP}}|$), with the incident THz radiation polarized perpendicular and parallel to ribbons, respectively. For incident light polarized perpendicular to the three-layer graphene ribbons, within a moderate gate voltage tuning range, i.e. ΔV_{gate} changing from 60 V to 120 V, the plasmonic resonance frequency varies in the range of \sim 210 cm⁻¹ to \sim 245 cm⁻¹, which is significantly wider than that of single-layer graphene ribbons of the same width (see Supporting Information S1). The lineshape of the plasmonic resonance exhibits the characteristic damped oscillator response which can be described by $\text{Im}(-f/(f^2 - f_p^2 + if\Gamma_p))$ with a plasmon damping rate of $\Gamma_p \approx 93 \text{ cm}^{-1}$ at $\Delta V_{\text{gate}} = 90 \text{ V}$. For incident light polarized parallel to the graphene ribbons, the transmission extinction monotonically increases with decreasing frequency and is well described by the Drude model for free carrier absorption, which for graphene is significant in the THz range. Figure 2(c) shows a comparison of the plasmonic resonances of four graphene ribbon arrays with different numbers of layers (i.e. 1 to 4 layers) at the same $\Delta V_{\rm gate} = 90$ V. The four structures have similar ribbon widths of about 1 um (their exact values are specified in the figure caption, and the differences are due to fabrication variation) and exactly the same periodicity of 2 µm. It is evident that the plasmonic resonance frequency increases significantly when the number of layers increases from one to three. The plasmonic resonance frequencies of the single-, double- and three-layer graphene ribbon arrays at $\Delta V_{\rm gate} = 90~{\rm V~are~173~cm^{-1},\,207~cm^{-1}}$ and 224 cm⁻¹, respectively. Compared to the results in the previous report,²⁸ our multilayer graphene structures show a considerably larger relative increase of the plasmonic resonance frequency (by ~30% for the three-layer structure) with respect to that of the single-layer structure. Although the resonance frequency of the four-layer structure

is also higher (by ~10%) than that of the three-layer structure, we find that this is mainly a result of the smaller ribbon width of the four-layer structure (which is ~0.95 μ m, about 20% smaller than the ~1.20 μ m ribbon width of the three-layer structure), as the graphene ribbon plasmonic resonance frequency is inverse proportional to the square root of the ribbon width (i.e. $f_p \propto w^{-1/2}$).

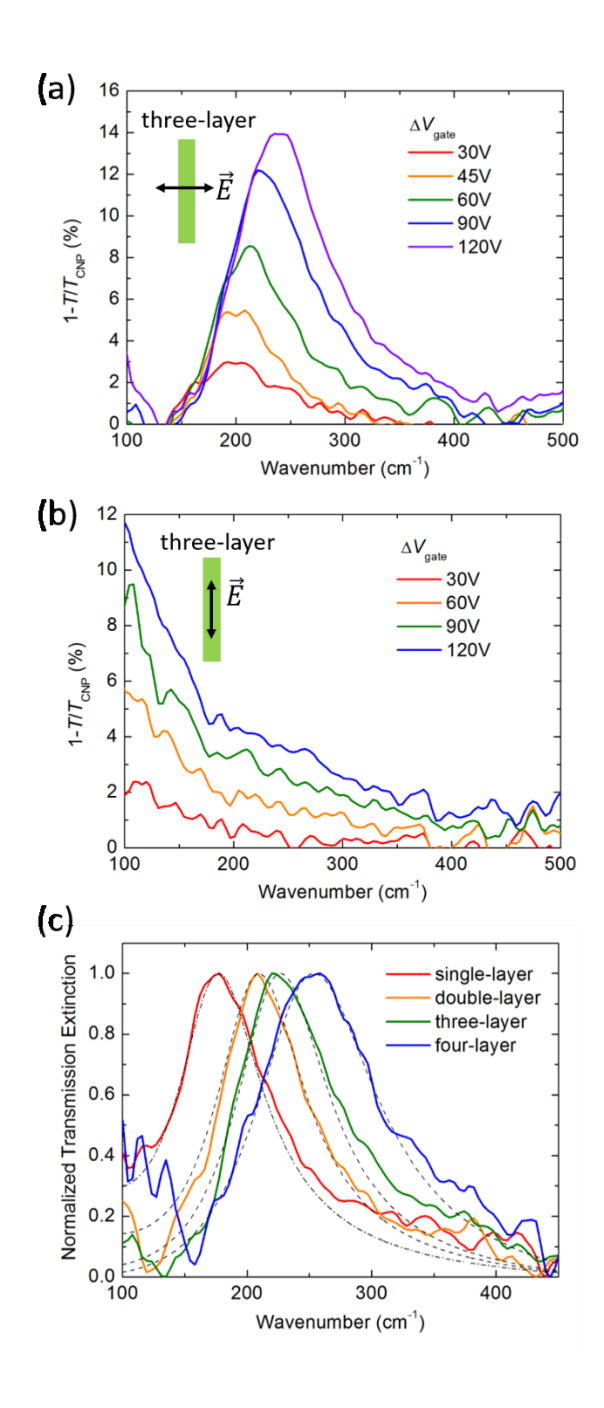


Figure 2. Experimental transmission extinction spectra of a three-layer graphene ribbon array at various back-gate voltages ($\Delta V_{\rm gate} = |V_{\rm gate} - V_{\rm CNP}|$), with the normally incident THz radiation polarized (a) perpendicular to the ribbons, and (b) parallel to the ribbons. (c) Normalized transmission extinction spectra associated with the plasmonic resonances of four different graphene ribbon arrays with the specified number of graphene layers at $\Delta V_{\rm gate} = 90$ V. All the graphene ribbon arrays have the same periodicity of 2 μm but somewhat different ribbon widths due to sample fabrication variation. The approximate average graphene ribbon widths for the single-layer to four-layer samples are 1.15 μm, 1.15 μm, 1.20 μm and 0.95 μm, respectively.

Figure 3(a) shows the extracted plasmonic resonance frequency versus total carrier density for the characterized samples with different numbers of graphene layers. For the single-layer graphene sample, the plasmonic resonance frequency is well fitted by the scaling law $f_p \propto |n|^{1/4}$ of massless Dirac fermions as indicated by the black dashed line, where n is the graphene carrier density. It is also evident that the plasmonic resonance frequencies of the multilayer graphene samples are significantly higher than that of the single-layer sample at any total carrier density. This is because that in the THz frequency range, the in-plane optical conductivity of each graphene layer is proportional to its Fermi energy, whereas the total optical conductivity of stacked multilayer graphene is the sum of the optical conductivity of each layer, as long as the thickness of the multilayer graphene is much smaller than the wavelength of interest. As the graphene Fermi energy E_F is proportional to \sqrt{n} , when a given total carrier density is distributed to several graphene layers, the total conductivity is larger than the conductivity of a single layer graphene with the same carrier density, i.e. $\sigma_{\text{multi}} \propto \Sigma_j \, E_{F,j} \propto \Sigma_j \, \sqrt{n_j} > \sigma_{\text{single}} \propto \sqrt{n_{\text{total}}}$ where j is the layer index and $\Sigma_j \, n_j = n_{\text{total}}$. Therefore, for the purpose of understanding the plasmonic

responses in the THz region, a multilayer graphene stack can be considered as a single-layer graphene with an effective Fermi energy E_F* higher than that determined by the total carrier density $(E_F \propto \sqrt{n_{\text{total}}})$. We have verified the accuracy of this theoretical approximation by comparing simulated transmission extinction spectra of single-layer and multilayer graphene ribbon arrays based on the finite difference time domain method (using Lumerical FDTD Solution). The transmission extinction spectrum associated with the plasmonic resonance of a multilayer graphene ribbon array with a few nm interlayer spacing is almost identical to that of a single-layer graphene ribbon array with a Fermi energy $E_F^* = \sum_j E_{F,j}$ (see Supporting Information S2). Therefore, by matching simulated transmission extinction spectra to the measured ones, we can obtain the effective Fermi energy \boldsymbol{E}_F^* of a multilayer graphene ribbon array at any total carrier density induced by the back-gate. The extracted effective Fermi energy E_F* versus total carrier density n_{total} of the four samples in Figure 3(a) are plotted in Figure 3(b), and Figure 3(c) shows the measured transmission extinction spectra of the three-layer graphene ribbon array in comparison with the matching simulated spectra. Evidently, the E_F of the double-layer and the three-layer structures are $\sim 40\%$ and $\sim 70\%$ higher than the E_F of the single-layer structure in the range of relatively high carrier densities. However, the E_F of the four-layer structure is also only \sim 70% higher than E_F, yielding little additional gain with respect to that of the three-layer structure.

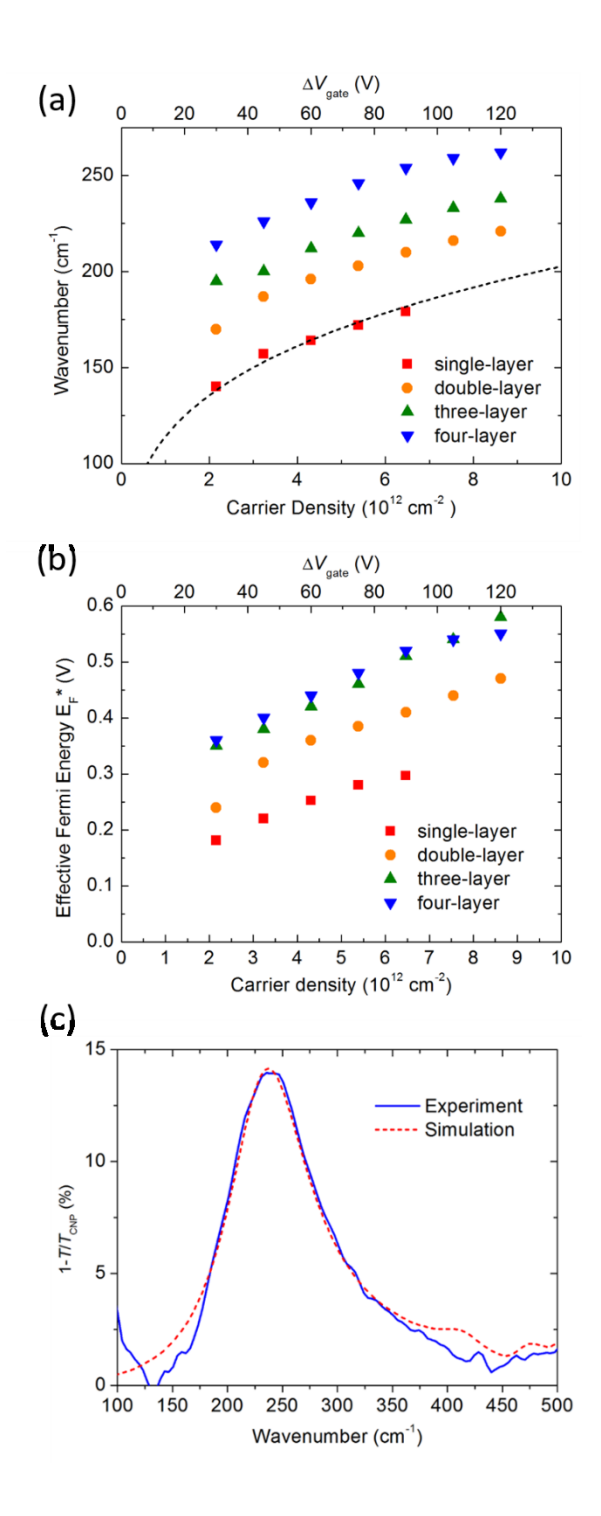


Figure 3. (a) Symbols are the plasmonic resonance frequency f_p (in terms of wavenumber) as a function of total gate-induced carrier density for each of the graphene ribbon arrays in Figure 2(c). The dashed line is the fit of the theoretical scaling law of single-layer graphene plasmonic resonance $f_p = A|n|^{1/4}$ to the single-layer sample's experimental data. **(b)** Extracted effective Fermi energy (E_F^*) as a function of total

gate-induced carrier density for each of the graphene ribbon arrays in Figure 2(c). (c) An example showing the extraction of the effective Fermi energy of a multilayer graphene ribbon array. The experimental transmission extinction spectrum of the three-layer graphene ribbon array at $\Delta V_{\text{gate}} = 120 \text{ V}$ matches the simulated transmission extinction spectrum of a single-layer graphene ribbon array of the same ribbon width and periodicity, and with its Fermi energy E_F set at 0.58 eV. Therefore, the effective Fermi energy E_F of the three-layer graphene ribbon array at $\Delta V_{\text{gate}} = 120 \text{ V}$ is $E_F^* = 0.58 \text{ eV}$.

As the effective Fermi energy \boldsymbol{E}_F^* is simply the sum of the Fermi energy in each graphene layer, to quantitatively understand the experimental observation, accurate knowledge on how the gate-controlled carrier density distributes in a multilayer graphene structure is needed. The previous work assumed that regardless of each layer's initial carrier density (e.g. due to unintentional doping), an applied gate voltage changes the Fermi energies of all the graphene layers by the same amount.²⁸ Under such an assumption, for an intrinsic multilayer graphene structure (i.e., the Fermi energy of each layer is initially at the Dirac point), an applied gate voltage would induce equal carrier density n_{total}/N in all the layers, which leads to an effective Fermi energy $E_F^* = \sqrt{N} \cdot E_F \, (E_F \propto \sqrt{n_{total}} \,)$ and hence a plasmonic resonance frequency increase by a factor of $\sqrt[4]{N}$. However, as we show in the following, this prediction is over-optimistic for multilayer graphene structures with $N \ge 3$. In fact, it has been shown that interlayer charge screening in stacked multilayer graphene is significant, ^{30,31} and therefore the first few layers closest to the gate obtain most of the gate-induced carrier density, whereas the other farther-away layers have negligible change. We take into account this interlayer charge screening effect to calculate the carrier density distribution in various multilayer graphene structures using the following model. We consider N layers of graphene laying on a $t_{\rm ox}$ =300 nm thick SiO₂ substrate with a dielectric constant $\varepsilon = 3.9$, and underneath the SiO₂ layer is the bulk Si back-gate. The interlayer distance between the j-th and the (j+1)-th layer is assumed to be $d_j = 3.5$ Å, j = 1...(N-1), and the distance between the SiO₂ substrate surface and the first graphene layer is also $d_0 = 3.5$ Å. The electrostatic potential of the Si back-gate V_g is swept from 0 to 150 V. We solve self-consistently the Poisson equations for the charge carrier density σ_j and the electrostatic potential φ_j of each layer (j = 1...N):

$$E_{\text{ox}} = \frac{V_{\text{g}} - \varphi_{\text{S}}}{t_{\text{ox}}}, \qquad E_{0} = \frac{\varphi_{\text{S}} - \varphi_{1}}{d_{0}},$$

$$E_{j} = \frac{\varphi_{j} - \varphi_{j+1}}{d_{j}}, \quad j = 1...(N-1)$$
(1)

where E_j is the normal component of the electric field above the j-th graphene layer, E_0 is the normal component of the electric field between the SiO₂ substrate surface and the first graphene layer, E_{0x} is the normal component of the electric field in the SiO₂ substrate, and φ_s is the electrostatic potential at the SiO₂ surface. The charge carrier desnity σ_j is found according to:

$$\varphi_j = \frac{\hbar v_F}{e} \sqrt{\frac{\pi |\sigma_j|}{e}} \times \frac{-\sigma_j}{|\sigma_i|} \tag{2}$$

where $v_{\rm F}=10^6$ cm/s is the graphene Fermi velocity. The 3N+3 variables are connected with one another by the equations above along with the boundary conditions $\varepsilon E_{\rm ox}=E_0$ at the SiO₂ surface, $E_N=0$ above the very top graphene layer, and for the electric fields above and below each graphene layer: $E_j-E_{j-1}=4\pi\sigma_j$, j=1...N (in CGS units).

Figure 4(a)-(b) show the calculated carrier density distributions as a function of back-gate voltage in the two-layer and three-layer graphene samples, respectively. It can be clearly seen that

the first (bottom) graphene layer always obtains the majority (>75%) of the total gate-induced carrier density, whereas in the three-layer structure, the third (top) layer only takes less than 10% of the total. For stacked multilayer graphene with even more layers, the carrier density share of the fourth layer and the higher layers combined (if any) is below 4% of the total, which has very limited influence on the total optical conductivity and hence the plasmonic resonance frequency of the multilayer graphene structure (see Supporting Information S3). The Fermi energy of each graphene layer can be calculated from the charge density distribution and the effective Fermi energy of the multilayer graphene structures can be obtained, which are plotted in Figure 4(c) and exhibit good agreement with the experimentally extracted values in Figure 3(b). We further calculate the plasmonic resonance frequency enhancement factor $(f_{\rm p,multi}/f_{\rm p,single})$ at a given total carrier density (e.g. 7.2×10^{12} cm⁻²) for different numbers of graphene layers, which are plotted in Figure 4(d). The prediction based on the model in the previous report is also plotted for comparison. Our calculation shows that both double-layer and three-layer graphene structures can significantly enhance the plasmonic resonance frequency. In contrast to the prediction of the previous model, our model also reveals that employing even more layers $(N \ge 4)$ can only lead to a small additional gain, which is in accordance with our experimental observation. It is important to note that the small additional gain predicted by our model for $N \ge 4$ may only apply to an ideal multilayer graphene structure, in which a graphene layer with a very small carrier density can still contribute to the total optical conductivity of the multilayer stack. However, the situation for a real device is more complicated, since for example a graphene layer with a relatively low Fermi energy likely has formation of microscopic charge puddles,³² which would not contribute to the total optical conductivity as predicted by our model.

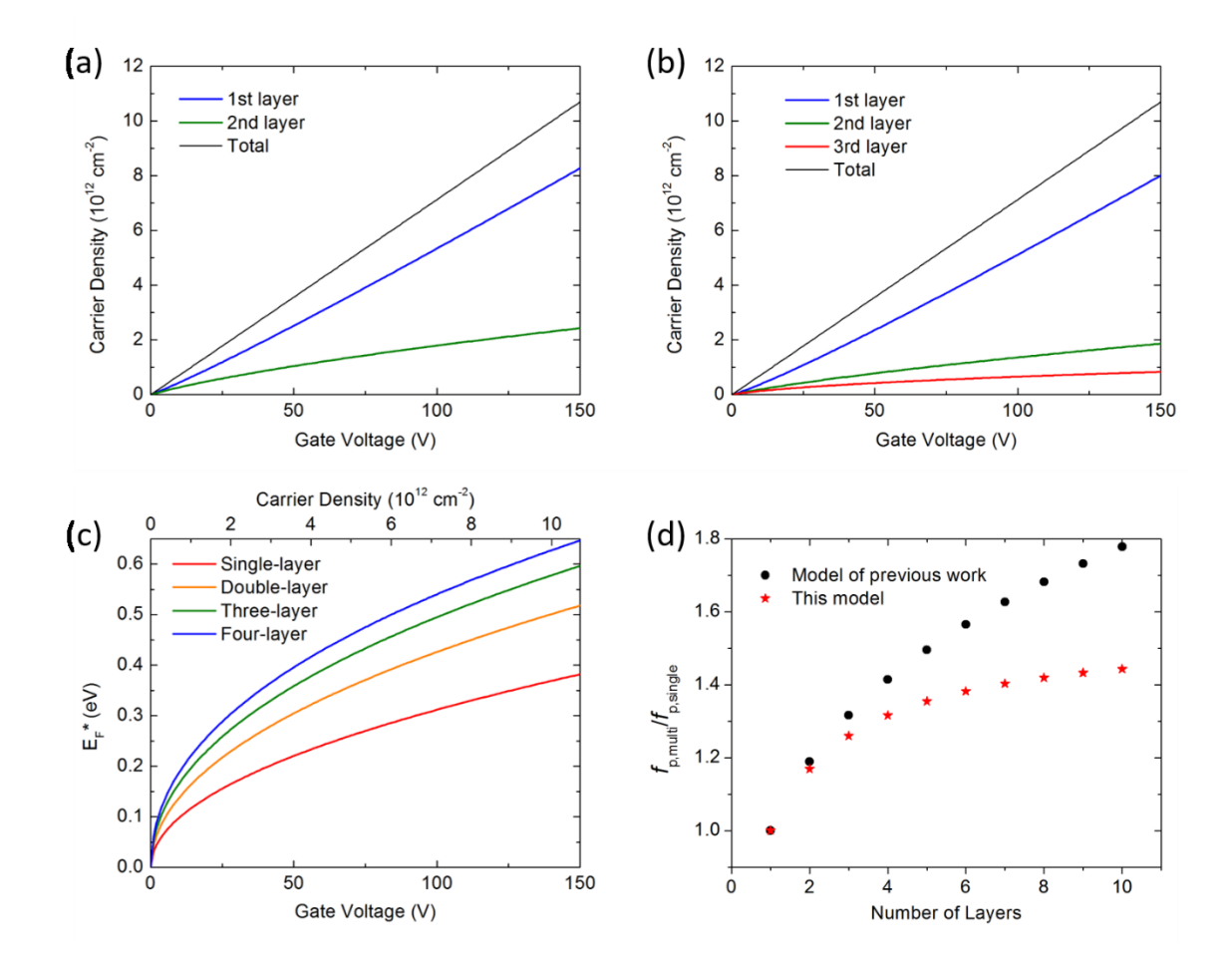


Figure 4. (a) Calculated carrier density distribution as a function of gate voltage in a double-layer graphene structure. (b) Calculated carrier density distribution as a function of gate voltage in a three-layer graphene structure. (c) Calculated effective Fermi energy E_F^* versus gate voltage (and carrier density) for graphene structures with 1 to 4 layers. (d) Calculated plasmonic resonance frequency enhancement factor $f_{p,multi}/f_{p,single}$ versus number of stacked graphene layers.

In summary, we have systematically studied the gate-tunable THz plasmonic resonances of graphene ribbon array structures containing different numbers of graphene layers. The multilayer graphene stack is realized by repeated transfer of single-layer graphene with random

alignment. Our experimental characterization demonstrate that within the same gate voltage range, both the plasmonic resonance frequency and its tuning range are significantly increased for the double-layer and the three-layer graphene structures, in comparison with those of the single-layer graphene structure. However, contrary to the prediction of a previous study, we find that employing even more graphene layers yields little additional benefit. These experimental observations are in good agreement with our theoretical model and calculation, which show that it is crucial to take into account the interlayer charge screening effect which leads to highly nonequal distributions of gate-induced carriers in different graphene layers. We find that for doublelayer and three-layer graphene structures, the non-equal distributions of gate-induced carriers lead to a significantly larger total optical conductivity (larger effective Fermi energy), which in turn produces a considerably higher plasmonic resonance frequency. However, for any additional graphene layer above the third layer, its share of the gate-induced carriers becomes negligible and therefore has little influence on the total optical conductivity. Our study provides new insights for designing and optimizing plasmonic structures based on multilayer graphene, which may exhibit crucial advantages over single-layer graphene plasmonic structures for a variety of photonic and optoelectronic device applications, such as modulators, sensors and detectors.

ASSOCIATED CONTENT

Supporting Information Available: Transmission Extinction Spectra of Graphene Ribbon Arrays with Different Numbers of Graphene Layers; Simulation of Transmission Extinction Spectra of Multilayer Graphene Ribbon Arrays; Calculated Carrier Distributions in Multilayer Graphene. The Supporting Information is available free of charge on the ACS Publications website at http://pubs.acs.org.

AUTHOR INFORMATION

Corresponding Authors

*E-mail: pqliu@buffalo.edu.

NOTES

The authors declare no competing financial interest.

ACKNOWLEDGMENTS

This work was partially supported by the National Science Foundation under the award number ECCS-1847203.

Reference

- 1. Novoselov, K. S.; Geim, A. K.; Morozov, S. V.; Jiang, D.; Zhang, Y.; Grigorieva, I. V.; Firsov, A. A. Electric field effect in atomically thin carbon films. *Science* **2004**, *306*, 666-669.
- 2. Ferrari, A. C. et al. Science and technology roadmap for graphene, related two-dimensional crystals, and hybrid systems. *Nanoscale* **2015**, *7*, 4598-4810.
- 3. Hwang, E. H.; Sarma, S. D. Dielectric function, screening, and plasmons in two-dimensional graphene. *Phys. Rev. B* **2007**, *75*, 205418.
- 4. Jablan, M.; Buljan, H.; Soljacic, M. Plasmonics in graphene at infrared frequencies. *Phys. Rev. B* **2009**, *80*, 245435.
- 5. Koppens, F. H. L.; Chang, D. E.; Garcia de Abajo, F. J. Graphene plasmonics: a platform for strong light–matter interactions. *Nano Lett.* **2011**, *11*, 3370-3377.

- Ju, L.; Geng, B.; Horng, J.; Girit, C.; Martin, M.; Hao, Z.; Bechtel, H. A.; Liang, X.; Zettl, A.;
 Shen, Y. R.; Wang, F. Graphene plasmonics for tunable terahertz metamaterials. *Nat. Nanotechnol.* 2011, 6, 630-634.
- 7. Nikitin, A. Y.; Guinea, F.; Garcia-Vidal, F. J.; Martin-Moreno, L. Surface plasmon enhanced absorption and suppressed transmission in periodic arrays of graphene ribbons. *Phys. Rev. B* **2012**, *85*, 081405.
- 8. Grigorenko, A.; Polini, M.; Novoselov, K. Graphene plasmonics. *Nat. Photonics* **2012**, *6*, 749-758.
- 9. Tassin, P.; Koschny, T.; Soukoulis, C. M. Graphene for terahertz applications. *Science* **2013**, *341*, 620-621.
- 10. Low, T.; Avouris, P. Graphene plasmonics for terahertz to mid-infrared applications. *ACS Nano* **2014**, *8*, 1086-1101.
- Liu, P. Q.; Luxmoore, I. J.; Mikhailov, S. A.; Savostianova, N. A.; Valmorra, F.; Faist, J.; Nash,
 G. R. Highly tunable hybrid metamaterials employing split-ring resonators strongly coupled to
 graphene surface plasmons. *Nat. Commun.* 2015, 6, 8969.
- 12. Rodrigo, D.; Limaj, O.; Davide Janner; Etezadi, D.; Abajo, F. J. G. d.; Pruneri, V.; Altug, H. Mid-infrared plasmonic biosensing with graphene. *Science* **2015**, *349*, 165-168.
- 13. Freitag, M.; Low, T.; Zhu, W.; Yan, H.; Xia, F.; Avouris, P. Photocurrent in graphene harnessed by tunable intrinsic plasmons. *Nat. Commun.* **2013**, *4*, 1951.
- 14. Chen, J.; Badioli, M.; Alonso-Gonzalez, P.; Thongrattanasiri, S.; Huth, F.; Osmond, J.; Spasenovic, M.; Centeno, A.; Pesquera, A.; Godignon, P.; Zurutuza Elorza, A.; Camara, N.; Garcia de Abajo, F. J.; Hillenbrand, R.; Koppens, F. H. L. Optical nano-imaging of gate-tunable graphene plasmons. *Nature* 2012, 487, 77-81.

- 15. Fei, Z.; Rodin, A. S.; Andreev, G. O.; Bao, W.; McLeod, A. S.; Wagner, M.; Zhang, L. M.; Zhao, Z.; Thiemens, M.; Dominguez, G.; Fogler, M. M.; Castro Neto, A. H.; Lau, C. N.; Keilmann, F.; Basov, D. N. Gate-tuning of graphene plasmons revealed by infrared nanoimaging. *Nature* 2012, 487, 82-85.
- Woessner, A.; Lundeberg, M. B.; Gao, Y.; Principi, A.; Alonso-Gonzalez, P.; Carrega, M.;
 Watanabe, K.; Taniguchi, T.; Vignale, G.; Polini, M.; Hone, J.; Hillenbrand, R.; Koppens, F.
 H. L. Highly confined low-loss plasmons in graphene–boron nitride heterostructures. *Nat. Mater.* 2015, 14, 421-425.
- 17. Iranzo, D. A.; Nanot, S.; Dias, E. J. C.; Epstein, I.; Peng, C.; Efetov, D. K.; Lundeberg, M. B.; Parret, R.; Osmond, J.; Hong, J.-Y.; Kong, J.; Englund, D. R.; Peres, N. M. R.; Koppens, F. H. L. Probing the ultimate plasmon confinement limits with a van der Waals heterostructure. *Science* 2018, 360, 291-295.
- Ni, G. X.; McLeod, A. S.; Sun, Z.; Wang, L.; Xiong, L.; Post, K. W.; Sunku, S. S.; Jiang, B.-Y.; Dean, C. R.; Fogler, M. M.; Basov, D. N. Fundamental limits to graphene plasmonics,
 Nature 2018, 557, 530-533.
- 19. Yan, H.; Li, X.; Chandra, B.; Tulevski, G.; Wu, Y.; Freitag, M.; Zhu, W.; Avouris, P.; Xia, F. Tunable infrared plasmonic devices using graphene/insulator stacks. *Nat. Nanotechnol.* **2012**, 7, 330-334.
- 20. Yan, H.; Low, T.; Zhu, W.; Wu, Y.; Freitag, M.; Li, X.; Guinea, F.; Avouris, P.; Xia, F. Damping pathways of mid-infrared plasmons in graphene nanostructures. *Nat. Photonics* 2013, 7, 394-399.
- 21. Brar, V. W.; Jang, M. S.; Sherrott, M.; Lopez, J. J.; Atwater, H. A. Highly Confined Tunable Mid-Infrared Plasmonics in Graphene Nanoresonators. *Nano Lett.* 2013, *13*, 2541-2547.

- 22. Fang, Z.; Thongrattanasiri, S.; Schlather, A.; Liu, Z.; Ma, L.; Wang, Y.; Ajayan, P. M.; Nordlander, P.; Halas, N. J.; Garcia de Abajo, F. J. Localized plasmons in nanostructured graphene. *ACS Nano* **2013**, *7*, 2388-2395.
- 23. Yeung, K. Y.; Chee, J.; Yoon, H.; Song, Y.; Kong, J.; Ham, D. Far-infrared graphene plasmonic crystals for plasmonic band engineering. *Nano Lett.* **2014**, *14*, 2479-2484.
- 24. Liu, P. Q.; Valmorra, F.; Maissen, C.; Faist, J. Electrically tunable graphene anti-dot array terahertz plasmonic crystals exhibiting multi-band resonances. *Optica* **2015**, *2*, 135-140.
- 25. Yan, H.; Low, T.; Guinea, F.; Xia, F.; Avouris, P. Tunable phonon-induced transparency in bilayer graphene nanoribbons. *Nano Lett.* **2014**, *14*, 4581-4586.
- 26. Fei, Z.; Iwinski, E. G.; Ni, G. X.; Zhang, L. M.; Bao, W.; Rodin, A. S.; Lee, Y.; Wagner, M.; Liu, M. K.; Dai, S.; Goldflam, M. D.; Thiemens, M.; Keilmann, F.; Lau, C. N.; Castro-Neto, A. H.; Fogler, M. M.; Basov, D. N. Tunneling plasmonics in bilayer graphene. *Nano Lett.* 2015, 15, 4973-4978.
- 27. Farmer, D. B.; Rodrigo, D.; Low, T.; Avouris, P. Plasmon-plasmon hybridization and bandwidth enhancement in nanostructured graphene. *Nano Lett.* **2015**, *15*, 2582-2587.
- 28. Rodrigo, D.; Tittl, A.; Limaj, O.; Garcia de Abajo, F. J.; Pruneri, V.; Altug, H. Double-layer graphene for enhanced tunable infrared plasmonics. *Light: Sci. Appl.* **2017**, *6*, e16277.
- 29. Emani, N. K.; Wang, D.; Chung, T.-F.; Prokopeva, L. J.; Kildishev, A. V.; Shalaev, V. M.; Chen, Y. P.; Boltasseva, A. Plasmon resonance in multilayer graphene nanoribbons. *Laser Photonics Rev.* 2015, 9, 650–655.
- 30. Datta, S. S.; Strachan, D.R.; Mele, E. J.; Johnson, A. T. C. Surface Potentials and Layer Charge Distributions in Few-Layer Graphene Films. *Nano Lett.* **2009**, *9*, 7-11.

- 31. Kuroda, M. A.; Tersoff, J.; Martyna, G. J. Nonlinear Screening in Multilayer Graphene Systems. *Phys. Rev. Lett.* **2011**, *106*, 116804.
- 32. Samaddar, S.; Yudhistira, I.; Adam, S.; Courtois, H., Winkelmann, C. B. Charge puddles in graphene near the Dirac point. *Phys. Rev. Lett.* **2016**, *116*, 126804.